Available online at www.sciencedirect.com

SciVerse ScienceDirect

Ceramics International 39 (2013) 6051–6056

CERAMICS INTERNATIONAL

www.elsevier.com/locate/ceramint

Enhancement of $Ca_3Co_4O_9$ thermoelectric properties by Cr for Co substitution

J.C. Diez[a], M.A. Torres[b], Sh. Rasekh[a], G. Constantinescu[a], M.A. Madre[a], A. Sotelo[a,*]

[a]*ICMA (UZ-CSIC), Departamento de Ciencia y Tecnología de Materiales y Fluidos, C/María de Luna 3, E-50018, Zaragoza, Spain*
[b]*Universidad de Zaragoza, Departamento de Ingeniería de Diseño y Fabricación, C/María de Luna 3, E-50018, Zaragoza, Spain*

Received 12 December 2012; received in revised form 8 January 2013; accepted 9 January 2013
Available online 17 January 2013

Abstract

$Ca_3Co_{4-x}Cr_xO_9$ polycristalline thermoelectric ceramics with small amounts of Cr have been synthesized by the classical solid state method. Microstructural characterizations have shown that all the Cr has been incorporated into the $Ca_3Co_4O_9$ structure and no Cr-containing secondary phases have been produced for Cr contents ≤ 0.05. Apparent density measurements have shown that all samples are very similar, with densities around 75% of the theoretical one. Electrical resistivity decreases and Seebeck coefficient slightly raises when Cr content increases until 0.05 Cr addition. The improvement in both parameters leads to higher power factor values than the usually obtained by conventional solid state routes.

Keywords: A. Powders: solid state reaction; A. Sintering; B. Platelets; C. Electrical properties; Thermopower

1. Introduction

Thermoelectric (TE) materials can transform a temperature difference to electrical power directly due to the well-known Seebeck effect. The conversion efficiency of such materials is quantified by the dimensionless figure of merit ZT, $TS^2/\rho\kappa$ (in which S^2/ρ is also called power factor, PF), where S is the Seebeck coefficient (or thermopower), ρ the electrical resistivity, κ the thermal conductivity, and T is the absolute temperature [1]. This important characteristic has focused attention on this type of materials in order to be applied as waste heat recovery devices [2] or solar thermoelectric generators [3]. Furthermore, they can also be used as heating/refrigeration devices [4].

Taking into account the above expression, high performance thermoelectric materials should possess large Seebeck coefficient and low electrical resistivity and thermal conductivity. Low electrical resistivity is necessary to minimize Joule heating, while a low thermal conductivity helps to maintain a large temperature gradient between the hot and cold sides in the thermoelectric device.

Nowadays TE devices based on intermetallic materials, such as Bi_2Te_3 or $CoSb_3$, with high ZT values at relatively low temperatures, are industrially used, e.g. in vehicles exhaust. However, due to their degradation at high temperatures under air, they cannot be applied in devices working in these conditions. These limitations were overwhelmed by the discovery in 1997 of attractive thermoelectrical properties in $Na_2Co_2O_4$ ceramics [5]. From the discovery of this thermoelectric oxide, much work has been performed on the cobaltite ceramics as promising thermoelectric materials for high temperature applications. Nowadays, research is focused on ceramic materials with relatively high thermoelectric performances, mainly on CoO-based materials, such as $Ca_3Co_4O_9$, $Bi_2Sr_2Co_{1.8}O_x$, and $Bi_2Ca_2Co_{1.7}O_x$ with interesting thermoelectric properties [6–9].

Crystallographic studies performed on those Co-based materials have demonstrated that they possess a monoclinic structure which is, in turn, composed of two different layers. These layers show an alternate stacking of a common conductive CdI_2-type hexagonal CoO_2 layer with a two-dimensional triangular lattice and a block layer

*Corresponding author. Tel.: +34 976762617; fax: +34 976761957.
E-mail address: asotelo@unizar.es (A. Sotelo).

0272-8842/$ - see front matter © 2013 Elsevier Ltd and Techna Group S.r.l. All rights reserved.
http://dx.doi.org/10.1016/j.ceramint.2013.01.021

composed of insulating rock-salt-type (RS) layers. The two sublattices (RS block and CdI_2-type CoO_2 layer) possess common *a*- and *c*-axis lattice parameters and β angles, but different *b*-axis length, causing a misfit along the *b*-direction [10,11]. Furthermore, it has also been found that the Seebeck coefficient values are governed by the incommensurability ratio and/or the charge of the RS block layer between the CoO_2 ones [9]. This is the basis for the modification of thermoelectric properties of a given material via chemical substitutions, as Gd and Y or Sb for Ca in $Ca_3Co_4O_9$ [12,13], Pb for Bi in $Bi_2Sr_2Co_{1.8}O_x$ or $Bi_2Ca_2Co_{1.7}O_x$ [14,15] or Ag additions in $Bi_2Sr_2Co_{1.8}O_x$ [16].

On the other hand, the high structural anisotropy of these materials leads to the formation of plate-like grains during the crystallization process. This shape anisotropy opens the route to align preferentially the grains using physical, mechanical and/or chemical processes. Such processes should allow the alignment of the conducting planes leading to macroscopic properties comparable to those obtained on single crystals. Numerous methods have been reported to be efficient to produce well aligned bulk materials, in these or in similar anisotropic systems, such as hot uniaxial pressing [17], spark plasma sintering [18], microwave texturing [19], laser floating zone melting (LFZ) [20], templated grain growth (TGG) [21], *etc*. The main advantage of these techniques is the production of materials with very high electrical properties due to the preferential conducting plane alignment with the conduction direction. On the other hand, they possess some drawbacks, as the high price of the spark plasma device and the relatively long processing time of the hot uniaxial pressing or the TGG. In the case of the processes involving samples melting, it has been reported that the electrical properties are strongly dependents on the growth speed [19,22–25].

The aim of this work is to study the effect of Cr for Co substitution on the microstructure and high temperature thermoelectric properties of $Ca_3Co_{4-x}Cr_xO_y$ prepared by the classical solid state synthetic route.

2. Experimental

$Ca_3Co_{4-x}Cr_xO_9$ polycristalline ceramic materials, with $x=0.00$, 0.01, 0.03, 0.05, and 0.10, were prepared by the conventional solid state route using commercial $CaCO_3$ (Panreac, 98+%), Co_2O_3 (Aldrich, 98+%), and Cr_2O_3 (Aldrich, 98+%) powders as starting materials. They were weighed in the appropriate proportions, well mixed and ball milled for 30 minutes at 300 rpm, in acetone media, in an agate ball mill. The obtained slurry has been heated under infrared radiation until all the acetone has been evaporated. The dry mixture was then manually milled in order to avoid the presence of agglomerates in the next steps. After milling, the homogeneous mixture was thermally treated twice at 750 and 800 °C for 12 h under air, with an intermediate manual milling in order to assure the total decomposition of carbonates, as reported previously [26]. After thermal treatment, the powders were uniaxially pressed at 400 MPa for 1 min in order to obtain green ceramic parallelepipeds (3 mm × 2.5 mm × 14 mm), with an adequate size for their thermoelectric characterization, which were subsequently sintered in the optimal conditions found in previous works, and consisting in one step heating at 900 °C for 24 h with a final furnace cooling [26].

Powder X-ray diffraction (XRD) patterns have been systematically recorded in order to identify the different phases in the thermoelectric sintered materials. Data have been collected at room temperature, with 2θ ranging between 5 and 60 degrees, using a Rigaku D/max-B X-ray powder diffractometer working with Cu Kα radiation. Apparent density measurements have been performed on several samples for each composition after sintering, using 4.677 g/cm^3 as theoretical density [27].

Microstructural observations were performed on fractured samples, using a JEOL 6000 scanning electron microscope, and on polished sections in a Field Emission Scanning Electron Microscope (FESEM, Carl Zeiss Merlin) fitted with an energy dispersive spectrometry (EDS) analyzer. Micrographs of polished sections of the samples have been used to analyze the different phases and their distribution. Electrical resistivity and Seebeck coefficient were simultaneously determined by the standard dc four-probe technique in a LSR-3 measurement system (Linseis GmbH), in the steady state mode and at temperatures ranging from 50 to 800 °C under He atmosphere. With the electrical resistivity and thermopower data, the power factor has been calculated in order to determine the samples performances. These properties have been compared with the results obtained in the undoped samples and with those reported in the literature at low temperatures (~50 °C), where oxygen diffusion is negligible, to avoid the influence of the atmosphere on the compared values.

3. Results and discussion

Powder XRD patterns for the different $Ca_3Co_{4-x}Cr_xO_9$ samples are displayed in Fig. 1 (from 5° to 40° for clarity). From these data, it is clear that all the samples have very similar diffraction patterns. As can be seen in Fig. 1a, corresponding to the undoped samples, all the peaks can be associated to the thermoelectric $Ca_3Co_4O_9$ phase, indicated by the reflection planes, and in agreement with previously reported data [28]. When Cr is added to the samples, two new peak appear at about 33° and 34° (indicated by ∗ in Fig. 1e), indicating the formation of a new phase, the $Ca_3Co_2O_6$ [28]. On the other hand, careful observation of these diagrams shows that there is no Cr-containing secondary phase which is a clear indication that Cr has entered into the $Ca_3Co_4O_9$ structure. This Cr incorporation into the $Ca_3Co_4O_9$ structure has no effect on the angles at what cobaltite peaks appear due to the very small difference in size between Co and Cr.

Fractographical observations have shown that all samples possess very similar microstructure. A representative

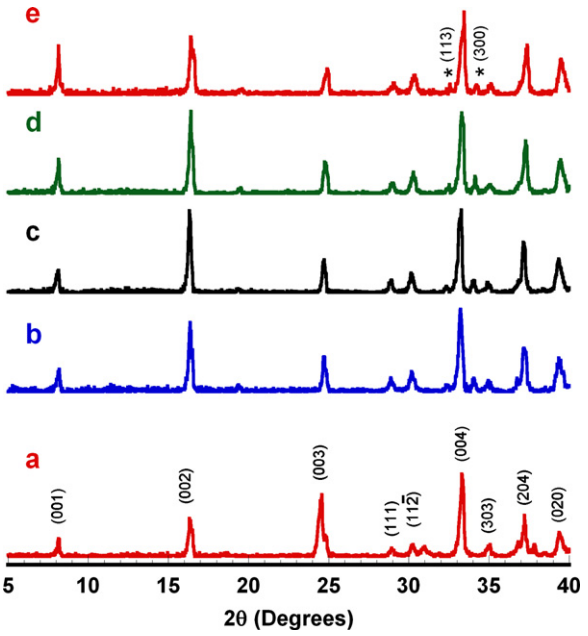

Fig. 1. Powder X-ray diffraction patterns obtained for the $Ca_3Co_{4-x}Cr_xO_9$ samples; $x=0.00$ (a); 0.01 (b); 0.03 (c); 0.05 (d); and 0.10 (e). The difraction planes indicate the $Ca_3Co_4O_9$ phase and the * the $Ca_3Co_2O_6$ one.

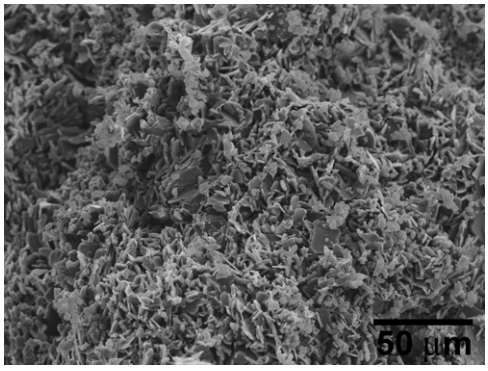

Fig. 2. SEM micrograph of a fractured surface of the 0.05 Cr-substituted sample showing the randomly oriented plate-like grains.

micrograph is displayed in Fig. 2 where a fracture, corresponding to the 0.05 Cr sample, is shown. In this figure it can be seen that the samples are composed by plate-like grains with different sizes, which is the typical microstructure for solid state synthesized $Ca_3Co_4O_9$ ceramic materials. Moreover, as expected from the used preparation techniques, the grains show no preferential orientation and they are randomly oriented.

SEM observations performed on polished sections have shown that all samples possess a relatively high degree of porosity, as illustrated in Fig. 3 where a general representative view of the 0.03 Cr sample is displayed. The porosity, together with the observations made for Fig. 2, are the typical trademarks for the solid state synthetic methods. Moreover, in this kind of materials, the reduction

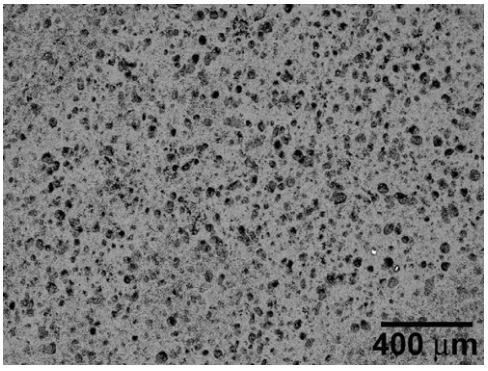

Fig. 3. General SEM micrograph performed on a polished section of the 0.03 Cr-substituted sample. Dark spots show the porosity in the bulk material.

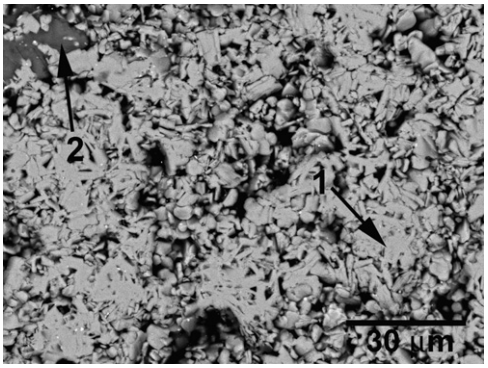

Fig. 4. Close view SEM micrograph performed on a polished section of the 0.10 Cr-substituted sample. Grey contrast corresponds to the $Ca_3Co_{4-x}Cr_xO_9$ and $Ca_3Co_2O_6$ phases (#1), while dark grey one is associated to the $Ca_{1-x}Cr_xO$ solid solution (#2).

of porosity in the classical solid state sintering process is a very difficult task due to the relatively low temperature stability of $Ca_3Co_4O_9$ phase (maximum stability temperature ~926 °C), compared with the minimum temperature to produce a liquid phase (~1350 °C) [28]. The great difference between both temperatures leads to a very slow densification process at the sintering temperatures (~900 °C), explaining the relatively high porosity obtained in these samples, as it has been already reported in previous works [26]. Furthermore, the apparent density measurements have shown that all samples posses very similar density (~75% of the theoretical density of $Ca_3Co_4O_9$ phase), indicating that Cr addition does not improve the densification in the solid state sintering processes.

When observing the samples in more detail, it has been found that major phase is the thermoelectric $Ca_3Co_4O_9$ one (grey contrast) in all cases, as illustrated in Fig. 4. This micrograph corresponds to the 0.10 Cr sample and shows all the secondary phases which can be observed in the $Ca_3Co_{4-x}Cr_xO_9$ samples. As it can be easily seen, the microstructure shows a relatively high level of porosity (as described previously) and the grey contrast as the major one. This contrast involves the $Ca_3Co_4O_9$ and $Ca_3Co_2O_6$

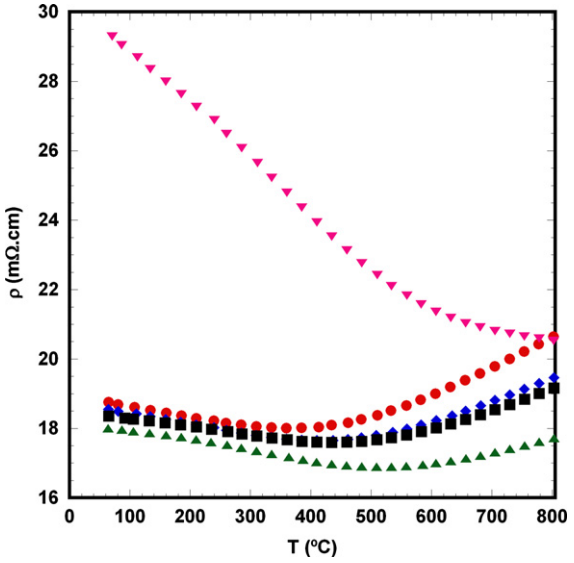

Fig. 5. Temperature dependence of the electrical resistivity, as a function of Cr content in $Ca_3Co_{4-x}Cr_xO_9$ samples, for $x=0.00$ (●); 0.01 (◆); 0.03 (■); 0.05 (▲); and 0.10 (▼).

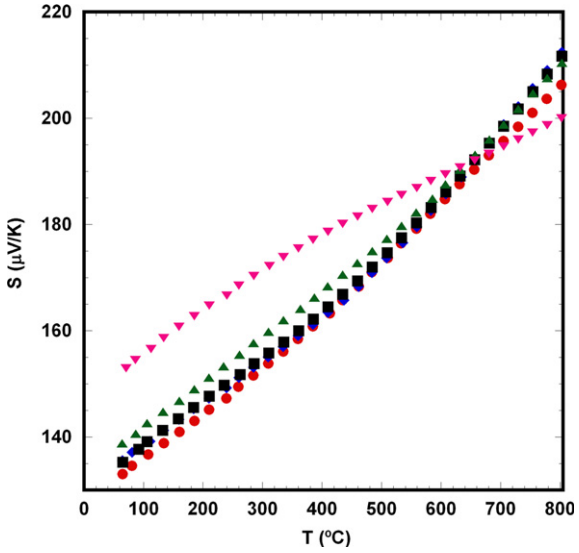

Fig. 6. Temperature dependence of the Seebeck coefficient as a function of Cr content in $Ca_3Co_{4-x}Cr_xO_9$ samples, for $x=0.00$ (●); 0.01 (◆); 0.03 (■); 0.05 (▲); and 0.10 (▼).

phases (indicated by #1), as they cannot easily be distinguished by their contrast. The other phase "appearing only in the 0.10 Cr samples" is the $Ca_{1-y}Cr_yO$ which can be observed in Fig. 4 as dark grey contrast (identified by #2). The formation of this phase can be explained by the EDS results which showed that until 0.05 Cr addition, all the Cr is found in the $Ca_3Co_{4-x}Cr_xO_9$ phase. Further Cr addition leads to a maximum Cr content in the $Ca_3Co_{4-x}Cr_xO_9$ phase of around 0.08, reaching its solubility limit in the synthetic conditions, and the remaining Cr produces the Ca–Cr–O solid solution.

The temperature dependence of electrical resistivity, as a function of the Cr content, is shown in Fig. 5. As can be clearly seen, the ρ (T) curves show a decrease of the measured resistivity from 0.00 to 0.05 Cr-substitution with a very similar behavior. These curves reflect a slope change at about 450 °C, from semiconducting-like ($d\rho/dT \leq 0$) to metallic-like ($d\rho/dT \geq 0$) one. In these samples, room temperature resistivity values slightly decrease when the Cr-substitution is increased. This effect is in agreement with the incorporation of Cr^{3+} cations in the CoO_2 layer [29] which produces the decrease in the resistivity values. On the other hand, samples with 0.10 Cr-substitution change radically the behavior to a semiconducting-like one in the whole measured temperature range. Moreover, the room temperature values are close to two times higher than the obtained for the rest of the samples. This different behavior is determined by the $Ca_{1-y}Cr_yO$ non-thermoelectric secondary phase found in these samples, compared with the lower doped ones. In any case, the lowest measured room temperature resistivity values (~18 mΩ cm for the 0.05 Cr-substituted samples) is around the best values obtained for $Ca_3Co_4O_9$ samples consolidated by spark plasma sintering (15–18 mΩ cm) [30].

Fig. 6 shows the variation of the Seebeck coefficient with the temperature, as a function of the Cr doping. In the plot, it can be clearly seen that the sign of the thermopower is positive for the entire measured temperature range, which confirms a conduction mechanism mainly governed by holes. The values of the Seebeck coefficient increase with temperature, with similar behavior for all the samples except for the 0.10 Cr-doped one, as already observed in the electrical resistivity measurements. The room temperature values increase with increasing the Cr contents from ~130 μV/K for the undoped samples to ~155 μV/K for the 0.10 Cr-doped one, slightly higher than those reported elsewhere (~125 μV/K) at the same temperature [31]. The maximum Seebeck coefficient value (~210 μV/K) at 800 °C, very close to the obtained for the undoped samples, is obtained for the samples with 0.01, 0.03 and 0.05 Cr-substitution. Moreover, S values at 625 °C (~190 μV/K) are also higher than the best values obtained for $Ca_3Co_4O_9$ samples consolidated by spark plasma sintering (170–175 μV/K) at the same temperature [30]. The similar values obtained for the undoped and the 0.01, 0.03 and 0.05 Cr-doped samples indicate that Cr addition does not affect, in a great extent, the $Ca_3Co_4O_9$ conduction band.

In order to evaluate the thermoelectric performances of these materials, the power factor has been calculated. The temperature dependence of the power factor, estimated from the data represented in Figs. 5 and 6 is plotted in Fig. 7. When considering PF values at around 50 °C (~room temperature), it can be clearly seen that the 0.01, 0.03 and 0.05 Cr-doped samples possess higher PF values than the undoped ones. The maximum increase is obtained for the 0.05 Cr-doped samples (~25% higher than the undoped ones). On the other hand, the 0.10

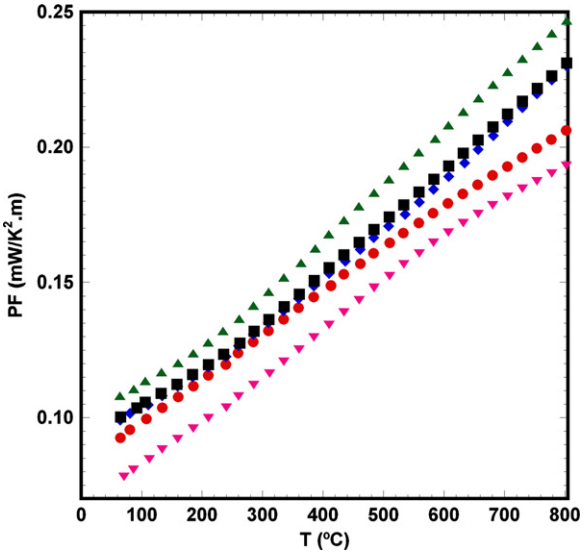

Fig. 7. Temperature dependence of the power factor as a function of Cr content in $Ca_3Co_{4-x}Cr_xO_9$ samples, for $x=0.00$ (●); 0.01 (◆); 0.03 (■); 0.05 (▲); and 0.10 (▼).

Cr-doped samples show the lowest PF values due to their high electrical resistivity. The highest PF value obtained at 800 °C (around 0.25 $mW/K^2.m$) for the 0.05 Cr-doped samples is higher than the highest values reported using the conventional solid state method (~0.18 mW/K^2 m) [29].

4. Conclusions

This paper demonstrates that Cr can substitute Co in $Ca_3Co_{4-x}Cr_xO_9$ in small proportions ($x \leq 0.05$) without modifying the crystal structure and improving the thermoelectric properties. Further Cr addition diminishes thermoelectric performances due to the formation of $Ca_{1-y}Cr_yO$ non-thermoelectric secondary phase. The optimal Cr for Co substitution has been determined using the values of the power factor at 50 and 800 °C, which is maximum for the 0.05 Cr-doped samples with values around 0.11 and 0.25 mW/K^2 m, respectively, which are about 25% higher than the obtained for the undoped samples. Moreover, the value at 800 °C is also higher than the typical ones obtained in samples prepared by the classical solid state method.

Acknowledgments

The authors wish to thank the Gobierno de Aragón (Research Groups T12 and T87) for financial support. The technical contributions of C. Estepa, and C. Gallego are also acknowledged. Sh. Rasekh also acknowledges a JAE-PreDoc 2010 grant from CSIC.

References

[1] D.M. Rowe, in: D.M. Rowe (Ed.), Thermoelectrics Handbook: Macro to Nano, 1st ed., CRC Press, Boca Raton, FL, 2006, pp. 1-3–1-7.
[2] G. Mahan, B. Sales, J. Sharp, Thermoelectric materials: new approaches to an old problem, Physics Today 50 (3) (1997) 42–47.
[3] H. Naito, Y. Kohsaka, D. Cooke, H. Arashi, Development of a solar receiver for a high-efficicency thermionic/thermoelectric conversion system, Solar Energy 58 (4–6) (1996) 191–195.
[4] C.M. Kim, Y.J. Hwang, Y.H. Ryu, Air conditioner for individual cooling/heating, US Patent US6393842, May 2002.
[5] I. Terasaki, Y. Sasago, K. Uchinokura, Large thermoelectric power in $NaCo_2O_4$ single crystals, Physical Review B 56 (20) (1997) 12685–12687.
[6] R. Funahashi, I. Matsubara, H. Ikuta, T. Takeuchi, U. Mizutani, S. Sodeoka, An oxide single crystal with high thermoelectric performance in air, Japanese Journal of Applied Physics 39 (11B) (2000) L1127–1129.
[7] M.A. Madre, Sh. Rasekh, J.C. Diez, A. Sotelo, New solution method to produce high performance thermoelectric ceramics: A case study of Bi–Sr–Co–O, Materials Letters 64 (23) (2010) 2566–2568.
[8] A. Sotelo, Sh. Rasekh, M.A. Madre, E. Guilmeau, S. Marinel, J.C. Diez, Solution-based synthesis routes to thermoelectric $Bi_2Ca_2Co_{1.7}O_x$, Journal of the European Ceramic Society 31 (9) (2011) 1763–1769.
[9] A. Maignan, D. Pelloquin, S. Hébert, Y. Klein, M. Hervieu, Thermoelectric power in misfit cobaltites ceramics: Optimization by chemical substitutions, Boletin de la Sociedad Espanola de Ceramica y Vidrio 45 (3) (2006) 122–125.
[10] A. Maignan, S. Hébert, M. Hervieu, C. Michel, D. Pelloquin, D. Khomskii., Magnetoresistance and magnetothermopower properties of Bi/Ca/Co/O and Bi(Pb)/Ca/Co/O misfit layer cobaltites, Journal of Physics: Condensed Matter 15 (17) (2003) 2711–2723.
[11] H. Itahara, C. Xia, J. Sugiyama, T. Tani, Fabrication of textured thermoelectric layered cobaltites with various rock salt-type layers by using β-$Co(OH)_2$ platelets as reactive templates, Journal of Materials Chemistry 14 (1) (2004) 61–66.
[12] H.Q. Liu, X.B. Zhao, T.J. Zhu, Y. Song, F.P. Wang, Thermoelectric properties of Gd, Y $Ca_3Co_4O_{9+\delta}$, Current Applied Physics 9 (2) (2009) 409–413.
[13] S. Demirel, M.A. Aksan, S. Altin, Low temperature electrical and thermal transport properties of the $Ca_{3-x}Sb_xCo_4O_9$ system, Journal of Materials Science: Materials in Electronics 23 (2012) 2251–2256.
[14] A. Sotelo, Sh. Rasekh, E. Guilmeau, M.A. Madre, M.A. Torres, S. Marinel, J.C. Diez, Improved thermoelectric properties in directionally grown $Bi_2Sr_2Co_{1.8}O_y$ ceramics by Pb for Bi substitution, Materials Research Bulletin 46 (12) (2011) 2537–2542.
[15] A. Sotelo, E. Guilmeau, Sh. Rasekh, M.A. Madre, S. Marinel, J.C. Diez, Enhancement of the thermoelectric properties of directionally grown Bi–Ca–Co–O through Pb for Bi substitution, Journal of the European Ceramic Society 30 (8) (2010) 1815–1820.
[16] A. Sotelo, M.A. Torres, G. Constantinescu, Sh. Rasekh, J.C. Diez, M.A. Madre, Effect of Ag addition on the mechanical and thermoelectric performances of annealed $Bi_2Sr_2Co_{1.8}O_x$ textured ceramics, Journal of the European Ceramic Society 32 (14) (2012) 3745–3751.
[17] V. Garnier, R. Caillard, A. Sotelo, G. Desgardin, Relationship among synthesis, microstructure and properties in sinter-forged Bi-2212 ceramics, Physica C 319 (3–4) (1999) 197–208.
[18] J.G. Noudem, D. Kenfaui, D. Chateigner, M. Gomina, Granular and lamellar thermoelectric oxides consolidated by spark plasma sintering, Journal of Electronic Materials 40 (5) (2011) 1100–1106.
[19] S. Marinel, D. Bourgault, O. Belmont, A. Sotelo, G. Desgardin, Microstructure and transport properties of YBCO zone melted samples processed in a microwave cavity and infra-red furnace, Physica C 315 (3–4) (1999) 205–214.
[20] A. Sotelo, E. Guilmeau, M.A. Madre, S. Marinel, J.C. Diez, M. Prevel, Fabrication and properties of textured Bi-based cobaltite thermoelectric rods by zone melting, Journal of the European Ceramic Society 27 (13–15) (2007) 3697–3700.
[21] M.M. Seabaugh, I.H. Kerscht, C.L. Messing, Texture development by templated grain growth in liquid-phase-sintered alpha-alumina, Journal of the American Ceramic Society 80 (5) (1997) 1181–1188.
[22] A. Sotelo, E. Guilmeau, M.A. Madre, S. Marinel, S. Lemmonier, J.C. Diez, $Bi_2Ca_2Co_{1.7}O_x$ thermoelectric ceramics textured by laser

floating zone method, Boletin de la Sociedad Espanola de Ceramica y Vidrio 47 (4) (2008) 225–228.
[23] J.C. Diez, E. Guilmeau, M.A. Madre, S. Marinel, S. Lemmonier, A. Sotelo, Improvement of $Bi_2Sr_2Co_{1.8}O_x$ thermoelectric properties by laser floating zone texturing, Solid State Ionics 180 (11–13) (2009) 827–830.
[24] Sh. Rasekh, G. Constantinescu, M.A. Torres, M.A. Madre, J.C. Diez, A. Sotelo, Growth rate effect on microstructure and thermoelectric properties of melt grown $Bi_2Ba_2Co_2O_x$ textured ceramics, Advances in Applied Ceramics 111 (8) (2012) 490–494.
[25] G. Constantinescu, Sh. Rasekh, M.A. Torres, M.A. Madre, J.C. Diez, A. Sotelo, Enhancement of the high-temperature thermoelectric performance of $Bi_2Ba_2Co_2O_x$ ceramics, Scripta Materialia 68 (1) (2013) 75–78.
[26] A. Sotelo, G. Constantinescu, Sh. Rasekh, M.A. Torres, J.C. Diez, M.A. Madre, Improvement of thermoelectric properties of $Ca_3Co_4O_9$ using soft chemistry synthetic methods, Journal of the European Ceramic Society 32 (10) (2012) 2415–2422.
[27] Y.C. Liou, W.C. Tsai, W.Y. Lin, U.R. Lee, Synthesis of $Ca_3Co_4O_9$ and $CuAlO_2$ ceramics of the thermoelectric application using a reaction-sintering process, Journal of the Australian Ceramic Society 44 (1) (2008) 17–22.
[28] E. Woermann, A. Muan, Phase equilibria in the system CaO–cobalt oxide in air, Journal of Inorganic and Nuclear Chemistry 32 (5) (1970) 1455–1459.
[29] S. Pinitsoontorn, N. Lerssongkram, N. Keawprak, V. Amornkitbamrung, Thermoelectric properties of transition metals-doped $Ca_3Co_{3.8}M_{0.2}O_{9+\delta}$ (M=Co, Cr, Fe, Ni, Cu and Zn), Journal of Materials Science: Materials in Electronics 23 (5) (2012) 1050–1056.
[30] D. Kenfaui, G. Bonnefont, D. Chateigner, G. Fantozzi, M. Gomina, J.G. Noudem, $Ca_3Co_4O_9$ ceramics consolidated by SPS process: Optimisation of mechanical and thermoelectric properties, Materials Research Bulletin 45 (9) (2010) 1240–1249.
[31] Y. Wang, Y. Sui, X. Wang, W. Su, X. Liu, Enhanced high temperature thermoelectric characteristics of transition metals doped $Ca_3Co_4O_{9+\delta}$ by cold high-pressure fabrication, Journal of Applied Physics 107 (3) (2010) 033708.